



Nonlinear tyre model-based sliding mode observer for vehicle state estimation

Hamza Ben Moussa¹ · Mohammed Bakhti¹

Received: 28 May 2023 / Revised: 2 January 2024 / Accepted: 5 January 2024 / Published online: 9 February 2024
© The Author(s), under exclusive licence to Springer-Verlag GmbH Germany, part of Springer Nature 2024

Abstract

A nonlinear sliding mode observer is proposed to estimate the lateral and longitudinal velocities and yaw rate of an automotive vehicle. The observer is based on standard outputs available in nowadays cars such as longitudinal and lateral accelerations, yaw rate, wheel rotational speed and steering angle. Tyre friction forces are described using the nonlinear Magic formula model, and the stability analysis is performed based on a Lyapunov quadratic function and the Sylvester criterion. The accuracy and the robustness of the observer are assessed by means of numerical simulation assuming very challenging driving scenarios and parameters uncertainties.

Keywords Lyapunov stability · Nonlinear tyre model · Sliding mode observer · Vehicle dynamics · Vehicle state estimation

List of symbols

Velocities/accelerations

v_x	Longitudinal vehicle velocity (m s^{-1})
v_y	Lateral vehicle velocity (m s^{-1})
r	Vehicle yaw rate (rd s^{-1})
ω_i	Wheel angular speed (rd s^{-1})
V_{xi}	Wheel coordinate system velocity (m s^{-1})
v_{xi}	Longitudinal velocity of the wheel center in the body-fixed coordinate system (m s^{-1})
v_{yi}	Lateral velocity of the wheel center in the body-fixed coordinate system (m s^{-1})
a_x	Longitudinal acceleration (m s^{-2})
a_y	Lateral acceleration (m s^{-2})

Forces acting on the vehicle

F_{xi}	Longitudinal tyre/road force (N)
F_{yi}	Lateral tyre/road force (N)

F_{ti}	Tyre traction/braking force (N)
F_{si}	Tyre lateral forces (N)
F_{zi}	Vertical load (N)

Magic formula parameters

B	Stiffness factor
D	Friction coefficient peak
E	Curvature factor

Tyre slip coefficient

λ_{xi}	Longitudinal slip
λ_{yi}	Lateral slip
α_i	The front left tyre slip angle (rd)

Vehicle parameters

m	Vehicle mass (kg)
h	Height of the vehicle center of gravity (CG) above the ground (m)
I_z	Vehicle moment of inertia around vertical axis (kg m^2)
l_f	Front wheelbase length (m)
l_r	Rear wheelbase length (m)
b_f	Front track width (m)

✉ Hamza Ben Moussa
benmoussa.hamza95@gmail.com

Mohammed Bakhti
m.bakhti@umi.ac.ma

¹ Moulay Ismail University, Ecole Nationale Supérieure d'arts et Métiers Meknès, Meknes, Morocco

b_r	Rear track width (m)
g	Gravitational constant (m s^{-2})
δ	Front steering angle (rd)
C	Common value of the shape factor
μ	Tyre/road friction coefficient

1 Introduction

Many control systems in nowadays cars, contribute to achieve good driving performances together with a comfortable and safe transportation. Safety is a key factor, and it must be guaranteed in different and/or unexpected driving conditions. One of the most critical aspects of transportation safety is the car stability that is most threatened when facing critical driving situations such as extreme steering manoeuvres, sudden tyre-road friction coefficient changing or emergency braking. To this end, an active control strategy is compulsory for a vehicle to improve steerability and to maintain the vehicle stability during critical situations.

Active safety systems generally rely on a real-time knowledge of the vehicle dynamic behaviour. The state (velocities and forces) of a vehicle cannot be completely supplied in a feedback scheme unless using very advanced and expensive sensors. Such devices are not suitable for production cars, and safety-relevant state variables must be then estimated based on common available car sensors.

Vehicle state estimation has been subject of investigation for numerous research papers. Using a GPS alongside with measured acceleration and yaw rate, supplied by inertial sensors, the state of the vehicle has been estimated using kinematic Kalman filter (KKF) [1] and nonlinear observers [2]. In [3], the integration of inertial navigation system sensors with GPS measurements demonstrated more accurate estimates of the vehicle states. Nevertheless, when an estimation scheme is based on GPS, it is usually penalized by the poor accuracy of usually implemented ones and their lack of reception in some geographical areas [4].

On the other hand, vehicle velocities can be estimated using road-tyre models with an observer based on friction lateral and longitudinal forces. In addition to an accurate tyre model, a good perception of the road condition is essential for such an estimation scheme to be efficient.

Kalman filters have been widely used in the literature to estimate either the vehicle state or parameters. This algorithm is based on the use of an adaptive square-root cubature Kalman filter and on the principle of similarities. A dual extended Kalman filter (DEKF) has been appraised in [5] when estimating the longitudinal and lateral states alongside the vehicle parameters. In [6–8], vehicle longitudinal and lateral velocities, yaw rate and tyre parameters have been estimated using extended Kalman filter (EKF), and in

[9], smooth variable structure filter (SVSF) has been used for the sideslip angle estimation to tackle modelling errors and enhance the estimation robustness. An unknown input observer was employed in [10] for estimating the lateral dynamics of the vehicle.

Unscented Kalman filters (UKF) have been introduced for the state estimation and vehicle's lateral dynamics estimation in [11, 12] respectively. In [11], a planar two-track model has been combined with the empiric tyre Magic formula to describe the vehicle and tyre behaviour. The accuracy has been increased with advanced vertical tyre load calculation considering tyre stiffness, and increases the estimation accuracy. In [12], a qualitative comparison between EKF and UKF has been presented. More recently, authors in [13] discussed a novel method for the side-slip angle and roll angle estimation based on EKF. They included to the basic EKF algorithm a fusion algorithm integrating side-slip angle rate to compensate the side-slip angle estimate. The estimation strategy demonstrated improved accuracy. An adaptive square root cubature Kalman filter (ASCKF)-based estimator has been proposed, in [14, 15], alongside an integral correction fusion algorithm to compensate the estimation error in the presence of coloured sensor noise.

Sliding mode observers (SMO) have also been suggested to address the vehicle state and/or parameters, estimation especially in the presence of external disturbances and/or parameters uncertainties. In [16, 17], a robust H_∞ SMO and a finite-frequency mixed H_-/H_∞ gain scheduling observer (GSO) have been suggested, respectively. The authors targeted an electric ground vehicle, yet they converted the nonlinear vehicle model to a linear parameter varying (LPV) form. In [18], a SMO has been compared to a linear vehicle model-based linear observer, extended Luenberger observer (ELO) and EKF.

However, all these studies, have simplified the observer design assuming linear tyre models.

Nonlinear models play a fundamental role in modelling complex systems, providing a more realistic approach to describing relationships that cannot be adequately represented by linear models [19–21]. To accurately describe the tyre behaviour, there are nonlinear empirical and physical models. A well-known model for the automotive engineering community is the Pacejka tyre model [22]. It is widely used, and it relies on the magic formula that describes the longitudinal force and side force based on the longitudinal slip and slip angle, respectively. The model is empirical, so its parameters strongly rely on experimental tyre data and may lack of accuracy. Unlike the empirical ones, physical tyre models, typically LuGre tyre model [23] and brush tyre model [24], can accurately describe the tyre behaviour. Nevertheless, their complex structure, including too many tyre parameters, makes their use very hard especially in real-time applications. A trade-off between accuracy and simplicity

may be achieved using semi-empirical nonlinear tyre model like the Dugoff one [25].

The main drawbacks of the above-mentioned observation techniques are their sensitiveness to parameters uncertainties. Furthermore, in the above-mentioned research papers, the observer/estimator stability analysis is rarely performed when nonlinear tyre models are assumed. In this paper, a sliding mode observer is proposed to estimate the longitudinal velocity, the lateral velocity, and the yaw rate for a four-wheel ground vehicle. The stability analysis is performed based on Lyapunov theory and the robustness of the observer is examined under a very challenging simulation scenario.

The rest of this paper are organized as follows. The four-wheel front steering vehicle is modelled in the next section. The dynamic equations of the rigid chassis are derived, and the tyre/road friction forces adopted model is presented. In Sect. 3, the SMO is designed. The estimation error dynamic is derived, and the stability analysis is performed using a Lyapunov quadratic function alongside with the Sylvester criterion. Simulation results and relevant discussion are presented in Sect. 4, while Sect. 5 concludes the paper.

2 Vehicle modelling

A schematic of the vehicle model used in this paper is sketched in Fig. 1. The vehicle body is assumed to be rigid, so suspension dynamics are neglected. The equations of motion are then derived using Newton’s rule.

The rigid body dynamics with respect to the centre of gravity (CoG) coordinate system can be written for longitudinal, lateral and yaw motions, respectively, as follows [26, 27]:

$$m\dot{v}_x = mv_yr + (F_{x1} + F_{x2} + F_{x3} + F_{x4}) \tag{1}$$

$$m\dot{v}_y = -mv_xr + (F_{y1} + F_{y2} + F_{y3} + F_{y4}) \tag{2}$$

$$I_z\dot{r} = \frac{b_f}{2} (F_{x1} - F_{x2}) + \frac{b_r}{2} (F_{x3} - F_{x4}) + l_f (F_{y1} + F_{y2}) - l_r (F_{y3} + F_{y4}) \tag{3}$$

This figure provides a detailed schematic of the 3-DOF vehicle model. Gray rectangles represent the wheels, with arrows indicating applied forces and associated distances. Vehicle velocity v and yaw rate r are depicted by arrows, and the x and y axes provide visual reference. This concise yet informative description aims to facilitate a clear understanding of the 3-DOF vehicle model.

In this paper, only front wheel steering δ is considered, so $\delta_1 = \delta_2 = \delta$, and $\delta_3 = \delta_4 = 0$. Tyre friction longitudinal forces F_{ti} and friction lateral forces F_{si} are related to the

longitudinal and lateral tyre forces as follows [26, 27]:

$$F_{x1} = F_{t1}\cos(\delta) - F_{s1}\sin(\delta) \tag{4}$$

$$F_{x2} = F_{t2}\cos(\delta) - F_{s2}\sin(\delta) \tag{5}$$

$$F_{x3} = F_{t3} \tag{6}$$

$$F_{x4} = F_{t4} \tag{7}$$

$$F_{y1} = F_{t1}\sin(\delta) + F_{s1}\cos(\delta) \tag{8}$$

$$F_{y2} = F_{t2}\sin(\delta) + F_{s2}\cos(\delta) \tag{9}$$

$$F_{y3} = F_{s3} \tag{10}$$

$$F_{y4} = F_{s4} \tag{11}$$

By combining the above equations, the dynamic model of the vehicle is as follows:

$$\begin{bmatrix} \dot{v}_x \\ \dot{v}_y \\ \dot{r} \end{bmatrix} = \begin{bmatrix} v_yr \\ -v_xr \\ 0 \end{bmatrix} + B_x(\delta)F_t + B_y(\delta)F_s \tag{12}$$

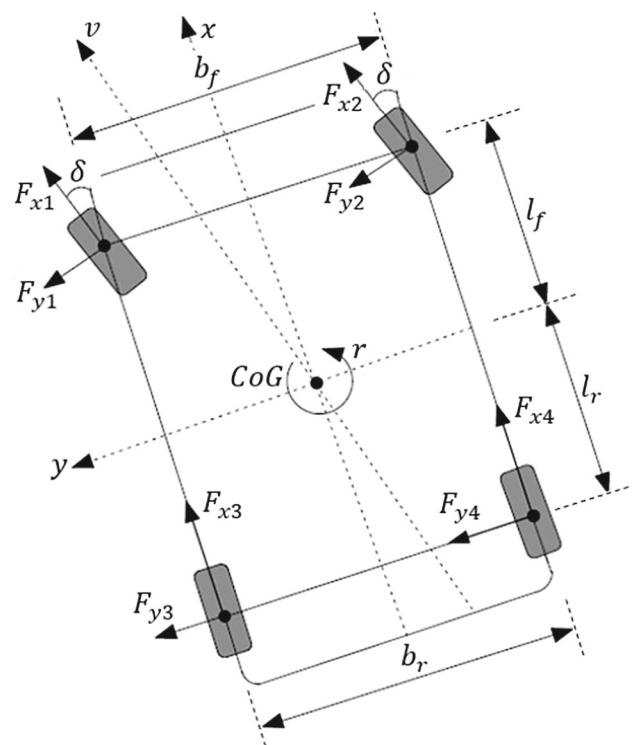


Fig. 1 Schematic of the 3-DOF vehicle model

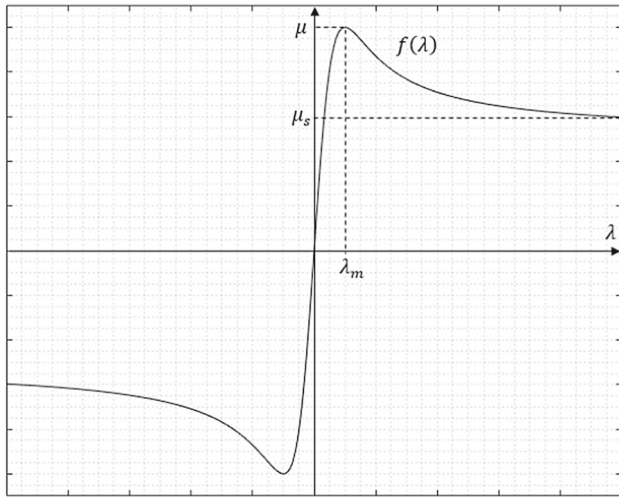


Fig. 2 Pacejka tyre model

where $F_t = [F_{t1} F_{t2} F_{t3} F_{t4}]^T$, $F_s = [F_{s1} F_{s2} F_{s3} F_{s4}]^T$,

$$B_x(\delta) = \begin{bmatrix} \frac{\cos(\delta)}{m} & \frac{\cos(\delta)}{m} & \frac{1}{m} & \frac{1}{m} \\ \frac{\sin(\delta)}{m} & \frac{\sin(\delta)}{m} & 0 & 0 \\ \frac{(l_f \sin(\delta) + \frac{b_f}{2} \cos(\delta))}{I_z} & \frac{(l_f \sin(\delta) - \frac{b_f}{2} \cos(\delta))}{I_z} & \frac{b_r}{2} & -\frac{b_r}{2} \end{bmatrix}$$

and

$$B_y(\delta_i) = \begin{bmatrix} \frac{-\sin(\delta)}{m} & \frac{-\sin(\delta)}{m} & 0 & 0 \\ \frac{\cos(\delta)}{m} & \frac{\cos(\delta)}{m} & \frac{1}{m} & \frac{1}{m} \\ \frac{(l_f \cos(\delta) - \frac{b_f}{2} \sin(\delta))}{I_z} & \frac{(l_f \cos(\delta) + \frac{b_f}{2} \sin(\delta))}{I_z} & -\frac{l_f}{2} & -\frac{l_f}{2} \end{bmatrix}$$

Friction longitudinal and lateral forces, F_{ti} and F_{si} , respectively, are calculated based on the Pacejka tyre model [22, 28] which we assume the same for the four wheels ($i = 1 \dots 4$) (cf. Fig. 2).

Figure 2 graphically represents the Pacejka tire model by depicting the variation of the friction coefficient μ with respect to the slip ratio λ . λ_m representing the slip ratio associated with the maximum friction coefficient, and μ_s , the asymptotic value of μ as λ approaches infinity. These points are vital in computing the parameters of the Pacejka model, including C, B, and E.

Friction forces depend on the longitudinal and lateral i th wheel slip ratios $\lambda_{xi} \lambda_{yi}$ respectively, and they are given by:

$$F_{ti} = F_{zi} f(\lambda_{xi}) \tag{13}$$

$$F_{si} = F_{zi} f(\lambda_{yi}) \tag{14}$$

where F_{zi} is the normal load on the i^{th} wheel, and:

$$f(\lambda) = \mu \sin(C \operatorname{atan}(B\lambda - E(B\lambda - \operatorname{atan}(B\lambda)))) \tag{15}$$

Pacejka tyre model parameters are defined as follows [22, 28]:

$$C = \frac{2}{\pi} \sin^{-1} \left(\frac{\mu_s}{\mu} \right) \tag{16}$$

$$B = \frac{\mu}{\lambda_m C} \tag{17}$$

$$E = \frac{B\lambda_m - \tan(\frac{\pi}{2C})}{B\lambda_m - \tan^{-1}(B\lambda_m)} \tag{18}$$

The normal load on a tyre is not only influenced by the vehicle weight. It also depends on the fore-aft location of the vehicle centre of gravity and longitudinal acceleration. For wheels 1 to 4, the normal loads are respectively given by [29]:

$$F_{z1} = \frac{m}{(l_f + l_r)} \left(0.5gl_r - 0.5\dot{v}_x h - \frac{l_r}{b_f} \dot{v}_y h \right) \tag{19}$$

$$F_{z2} = \frac{m}{(l_f + l_r)} \left(0.5gl_r - 0.5\dot{v}_x h + \frac{l_r}{b_f} \dot{v}_y h \right) \tag{20}$$

$$F_{z3} = \frac{m}{(l_f + l_r)} \left(0.5gl_f + 0.5\dot{v}_x h - \frac{l_f}{b_r} \dot{v}_y h \right) \tag{21}$$

$$F_{z4} = \frac{m}{(l_f + l_r)} \left(0.5gl_f + 0.5\dot{v}_x h + \frac{l_f}{b_r} \dot{v}_y h \right) \tag{22}$$

Longitudinal and lateral slip ratios are given by [2]:

$$\lambda_{xi} = \frac{(\omega_i R_w - V_{xi})}{V_{xi}} \tag{23}$$

$$\lambda_{yi} = \sin(\alpha_i) \tag{24}$$

where V_{xi} , the velocities in x-direction of the wheel coordinate systems, and α_i , the tyre slip angle, are respectively given by [2]:

$$V_{xi} = \sqrt{(v_{xi}^2 + v_{yi}^2)} \cos(\alpha_i) (i = 1, \dots, 4) \tag{25}$$

$$\alpha_i = \delta_i - \tan^{-1} \left(\frac{v_{yi}}{v_{xi}} \right) (i = 1, \dots, 4) \tag{26}$$

The longitudinal and lateral velocities at the wheel centre relatively to the body-fixed coordinate system are given by:

$$v_{x1} = v_x - \frac{r b_f}{2} \tag{27}$$

$$v_{y1} = v_y - r l_f \tag{28}$$

$$v_{x2} = v_x + \frac{r b_f}{2} \tag{29}$$

$$v_{y2} = v_y + rl_f \tag{30}$$

$$v_{x3} = v_x - \frac{rb_r}{2} \tag{31}$$

$$v_{y3} = v_y - rl_r \tag{32}$$

$$v_{x4} = v_x + \frac{rb_r}{2} \tag{33}$$

$$v_{y4} = v_y - rl_r \tag{34}$$

Finally, the i^{th} wheel rotational speed is related to the traction/braking respective torque T_i as follows:

$$I_z \dot{\omega}_i = T_i - F_{xi} R_w (i = 1, \dots, 4) \tag{35}$$

$$M_z = \frac{b_f}{2} (F_{x1} - F_{x2}) + \frac{b_r}{2} (F_{x3} - F_{x4}) + l_f (F_{y1} + F_{y2}) - l_r (F_{y3} + F_{y4}) \tag{38}$$

The vehicle dynamics are then written as follows:

$$\dot{v}_x = v_y r + a_x \tag{39}$$

$$\dot{v}_y = -v_x r + a_y \tag{40}$$

$$\dot{r} = \frac{M_z}{I_z} \tag{41}$$

In this paper, we propose and analyse the following observer:

3 Sliding mode observer design

In this section, a nonlinear sliding mode observer is proposed to give an estimation for the vehicle’s longitudinal and lateral velocities v_x and v_y , as well as yaw rate r . The observer design is based on the dynamic model derived in the previous section and lies on the following assumptions:

Assumption 1 The vehicle longitudinal acceleration a_x , lateral acceleration a_y , yaw rate r , wheel speeds ω_i and front-wheel steering δ are available outputs.

Assumption 2 The tyre-road friction coefficient for each wheel $\mu_i (i = 1, \dots, 4)$ is known.

Both assumptions are reasonable since lateral acceleration and yaw rate are available outputs via appropriate sensors in cars equipped with electronic stability program (ESP), and longitudinal acceleration is obtained with a separate inertial measurement unit (IMU) [2, 30, 31]. The tyre-road friction coefficient can be measured or estimated as discussed in [32, 33].

Let:

$$F_x = \sum_{i=1}^4 F_{xi} = ma_x \tag{36}$$

$$F_y = \sum_{i=1}^4 F_{yi} = ma_y \tag{37}$$

$$\hat{v}_x = \hat{v}_y r + a_x - k_{v_x} \text{sign}(F_x - \hat{F}_x) \tag{42}$$

$$\hat{v}_y = -\hat{v}_x r + a_y - k_{v_y} \text{sign}(F_y - \hat{F}_y) \tag{43}$$

$$\hat{r} = \frac{\hat{M}_z}{I_z} + k_r \text{sign}(r - \hat{r}) \tag{44}$$

Using the vehicle/observer dynamic Eqs. (39) to (44), the observation error dynamics are then given by:

$$\tilde{v}_x = \tilde{v}_y r + k_{v_x} \text{sign}(F_x - \hat{F}_x) \tag{45}$$

$$\tilde{v}_y = -\tilde{v}_x r + k_{v_y} \text{sign}(F_y - \hat{F}_y) \tag{46}$$

$$\tilde{r} = \frac{1}{I_z} (M_z - \hat{M}_z) - k_r \text{sign}(\tilde{r}) \tag{47}$$

where $\tilde{v}_x = v_x - \hat{v}_x$, $\tilde{v}_y = v_y - \hat{v}_y$ and $\tilde{r} = r - \hat{r}$.

The observer stability is discussed using the following quadratic Lyapunov function:

$$V = \frac{1}{2} (\tilde{v}_x^2 + \tilde{v}_y^2 + \tilde{r}^2) \tag{48}$$

The Lyapunov function time derivative along the trajectories (45)–(47) is given by:

$$\begin{aligned} \dot{V} = & k_{v_x} \text{sign}(F_x - \widehat{F}_x) \tilde{v}_x + k_{v_y} \text{sign}(F_y - \widehat{F}_y) \tilde{v}_y \\ & + \tilde{r} \frac{(M_z - \widehat{M}_z)}{I_z} - k_r \text{sign}(\tilde{r}) \tilde{r} \end{aligned} \tag{49}$$

To demonstrate the negative definiteness of the above-mentioned Lyapunov function time derivative, we use the approximate signum function $\text{sign}_{\text{apr}}(x)$ defined as follows:

$$\text{sign}_{\text{apr}}(x) = \frac{x}{|x| + \eta} \tag{50}$$

where η is a small positive scalar.

Define also:

$$k_x = \frac{k_{v_x}}{|F_x - \widehat{F}_x| + \eta} \tag{51}$$

$$k_y = \frac{k_{v_y}}{|F_y - \widehat{F}_y| + \eta} \tag{52}$$

$$k_{rr} = \frac{k_r}{|r - \widehat{r}| + \eta} \tag{53}$$

The time derivative of the Lyapunov function is then:

$$\dot{V} = k_x(F_x - \widehat{F}_x)\tilde{v}_x + k_y(F_y - \widehat{F}_y)\tilde{v}_y + \tilde{r} \frac{(M_z - \widehat{M}_z)}{I_z} - k_{rr}\tilde{r}^2 \tag{54}$$

Based on the friction forces model, as discussed in [2], there exist positive constants $c_i, i = 1, \dots, 9$, such that:

$$(F_x - \widehat{F}_x)\tilde{v}_x \leq -c_1\tilde{v}_x^2 + c_2|\tilde{v}_x||\tilde{v}_y| + c_3|\tilde{v}_x||\tilde{r}| \tag{55}$$

$$(F_y - \widehat{F}_y)\tilde{v}_y \leq c_4|\tilde{v}_y||\tilde{v}_x| - c_5\tilde{v}_y^2 + c_6|\tilde{v}_y||\tilde{r}| \tag{56}$$

$$\tilde{r} \frac{(M_z - \widehat{M}_z)}{I_z} \leq c_7|\tilde{v}_x||\tilde{r}| + c_8|\tilde{v}_y||\tilde{r}| + c_9\tilde{r}^2 \tag{57}$$

Using (54) and (55)–(57), we have:

$$\begin{aligned} \dot{V} \leq & k_x(-c_1\tilde{v}_x^2 + c_2|\tilde{v}_x||\tilde{v}_y| + c_3|\tilde{v}_x||\tilde{r}|) \\ & + k_y(c_4|\tilde{v}_y||\tilde{v}_x| - c_5\tilde{v}_y^2 + c_6|\tilde{v}_y||\tilde{r}|) \\ & + (c_7|\tilde{v}_x||\tilde{r}| + c_8|\tilde{v}_y||\tilde{r}| + c_9\tilde{r}^2) - k_{rr}\tilde{r}^2 \leq \tilde{x}^T Q \tilde{x} \end{aligned} \tag{58}$$

where $\tilde{x} = [\tilde{v}_x \ \tilde{v}_y \ \tilde{r}]^T$, and

$$Q = \begin{bmatrix} -k_x c_1 & \frac{1}{2}(k_x c_2 + k_y c_4) & \frac{1}{2}(k_x c_3 + c_7) \\ \frac{1}{2}(k_x c_2 + k_y c_4) & -k_y c_5 & \frac{1}{2}(k_y c_6 + c_8) \\ \frac{1}{2}(k_x c_3 + c_7) & \frac{1}{2}(k_y c_6 + c_8) & c_9 - k_{rr} \end{bmatrix} \tag{59}$$

According to the well-known Sylvester criterion, matrix Q is negative definite if and only if all its leading principal minors are negative.

The first principal minor of Q is $-k_x c_1$, so k_x must be positive. The second principal minor is given by:

$$\begin{aligned} & k_x c_1 k_y c_5 - \frac{1}{4}(k_x c_2 + k_y c_4)^2 \\ & = k_x c_1 k_y c_5 - \frac{1}{4}(k_x^2 c_2^2 + k_y^2 c_4^2 + 2k_x c_2 k_y c_4) \\ & = -\frac{1}{4}\left(k_y^2 c_4^2 + 2k_y c_4 \frac{k_x(c_2 c_4 - 2c_1 c_5)}{c_4} + k_x^2 c_2^2\right) \\ & = -\frac{1}{4}\left(k_y c_4 + \frac{k_x(c_2 c_4 - 2c_1 c_5)}{c_4}\right)^2 \\ & - \frac{k_x^2}{4}\left(c_2^2 - \left(\frac{c_2 c_4 + 2c_1 c_5}{c_4}\right)^2\right) < 0 \end{aligned} \tag{60}$$

So:

$$\begin{aligned} & \frac{1}{4}\left(k_y c_4 + \frac{k_x(c_2 c_4 - 2c_1 c_5)}{c_4}\right)^2 \\ & > \frac{k_x^2}{4}\left(\left(\frac{c_2 c_4 + 2c_1 c_5}{c_4}\right)^2 - c_2^2\right) \end{aligned} \tag{61}$$

And:

$$k_y > \frac{k_x}{c_4} \left(\sqrt{\left(\frac{c_2 c_4 + 2c_1 c_5}{c_4}\right)^2 - c_2^2} - \frac{c_2 c_4 - 2c_1 c_5}{c_4} \right) \tag{62}$$

The third principal minor, which is the matrix determinant, is given by:

$$\begin{aligned} \det(Q) = & -k_x c_1 \left(-k_y c_5 (c_9 - k_{rr}) - \frac{1}{4}(k_y c_6 + c_8)^2 \right) \\ & - \frac{1}{2}(k_x c_2 + k_y c_4) \left(\frac{1}{2}(k_x c_2 + k_y c_4)(c_9 - k_{rr}) \right. \\ & \left. - \frac{1}{4}(k_y c_6 + c_8)(k_x c_3 + c_7) \right) \\ & + \frac{1}{2}(k_x c_3 + c_7) \left(\frac{1}{4}(k_x c_2 + k_y c_4)(k_y c_6 + c_8) \right) \end{aligned}$$

$$-\frac{1}{2}(k_x c_3 + c_7)k_y c_5 \tag{63}$$

After some tedious calculation, one can notice that the determinant may be made negative by choosing k_{rr} large enough.

4 Simulation results

4.1 General model description

In this section, we provide a detailed description of the organizational structure of the three-degrees-of-freedom (3-DOF) vehicle dynamics model and the associated sliding mode observer. The organizational chart offers a visual representation of the internal framework of the model, elucidating key components and their interconnections. This preliminary overview aims to furnish readers with a profound understanding of how the model is articulated before delving into the analysis of simulation results. The following figure illustrates the organizational chart, facilitating a visual grasp of the model’s complexity.

Figure 3 provides a detailed depiction of the organizational chart for the three-degrees-of-freedom (3-DOF) vehicle dynamics model, incorporating both the Pacejka tire model and the sliding mode observer. The system’s inputs are represented by the steering angle, traction or braking torque, and the friction coefficient. The observer algorithm utilizes longitudinally and laterally measured accelerations, along with wheel speed, as parameters. These variables can be easily obtained through typical sensors. The arrowed connections in the figure illustrate the interactions and information exchanges among these components, offering a comprehensive view of the model’s internal structure. This visual representation is carefully crafted to enhance understanding, paving the way for a detailed analysis of simulation results.

4.2 Accuracy of the observer

In this section, the performance of the proposed sliding mode observer developed in the previous section is appraised by means of numerical simulation.

The longitudinal acceleration a_x , lateral acceleration a_y , yaw rate r , wheel speeds ω_i and front-wheel steering δ are available outputs, and the observed state is:

$$\hat{x} = [\hat{v}_x \hat{v}_y \hat{r}]^T \tag{64}$$

The observer algorithm has been implemented in Matlab/Simulink environment with a small step time for numerical integration to deal with the system nonlinearities. The

Table 1 Numerical parameters adopted for simulation

Vehicle parameters			
$m = 1298.9 \text{ kg}$	$h = 0.6 \text{ m}$	$I_z = 1627 \text{ kg.m}^2$	
$l_f = 1 \text{ m}$	$l_r = 1.454 \text{ m}$	$b_f = 1.436 \text{ m}$	$b_r = 1.436 \text{ m}$
Tyre/road parameters			
$I_w = 2.1 \text{ kg.m}^2$	$R_w = 0.35 \text{ m}$	$\mu = 1(\text{Dry asphalt})$	$\mu = 0.5(\text{Icy road})$
Magic formula parameters			
$B = 12.12$	$C = 1.65$		$E = -0.5804$
Observer parameters			
$k_{v_x} = 5$	$k_{v_y} = 0.8$		$k_r = 30$

step time has been set to $T_s = 5.10^{-6} \text{ s}$. The nominal vehicle model used for the simulation is based on the Magic formula tyre model, and Table 1. Shows the numerical parameters that have been adopted.

Initial states for the nominal plant and for the observer are set to:

$$x_0 = [v_{x0} \ v_{y0} \ r_0]^T = [27.78\text{m.s}^{-1} \ 0 \ 0]^T \tag{65}$$

$$\hat{x}_0 = [\hat{v}_{x0} \ \hat{v}_{y0} \ \hat{r}_0]^T = [22.22\text{m.s}^{-1} \ 0.5\text{m.s}^{-1} \ 0.5\text{rd.s}^{-1}]^T \tag{65}$$

During time interval $[0, 15\text{s}]$, the performance of the observer is examined. First, the vehicle is performing a lane change manoeuvre depicted in Fig. 4. Then, during time interval $[4, 6\text{s}]$, the braking/accelerating torque shown in Fig. 5 is applied to the corresponding wheels. For time interval $[6, 15\text{s}]$ a μ - split scenario is introduced simultaneously with a lane change, while the vehicle is braking. Such a scenario assumes different contact surfaces for left and right vehicle tyres. For the tyres on a dry asphalt road, the tyre–road friction coefficient is assumed to be of constant value ($\mu = 1$), and at time $t = 6\text{s}$, it steps to ($\mu = 0.5$) for the right wheels (cf. Fig. 6).

This figure illustrates the graphical representation of the steering angle for the four wheels of the vehicle. Each wheel is associated with a specific angle, depicting the configuration of the steering system. This visualization provides a clear understanding of how the wheels respond and contribute to the overall manoeuvrability of the vehicle.

Figure 5 Detailed the graphical profiles of braking and accelerating torques for the four wheels of the vehicle. Each wheel displays its individual profile. This visualization provides a detailed understanding of how these torques act individually on each wheel, influencing the deceleration and acceleration dynamics of the vehicle

Fig. 3 General Model Description

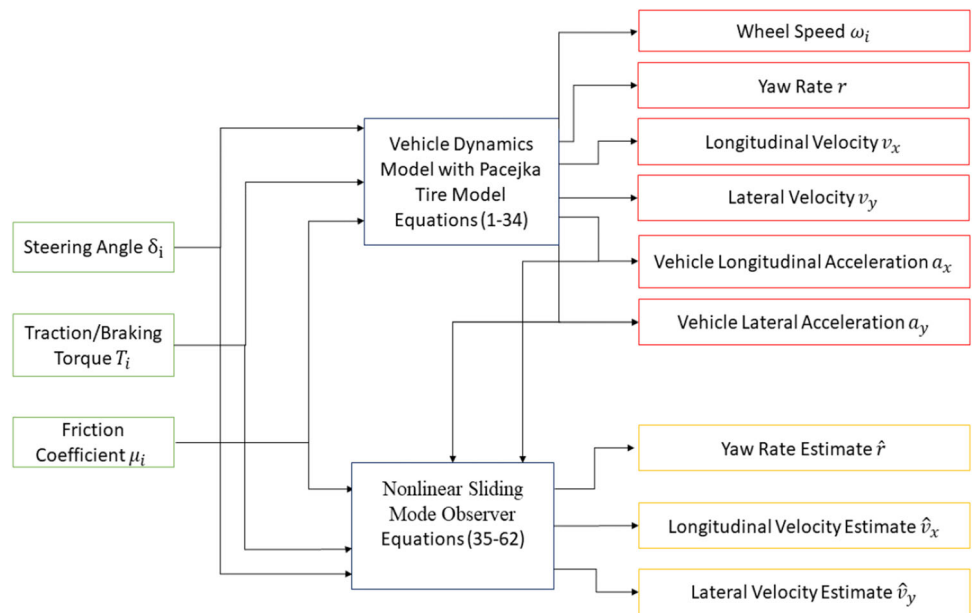


Fig. 4 The steering angle for the four wheels

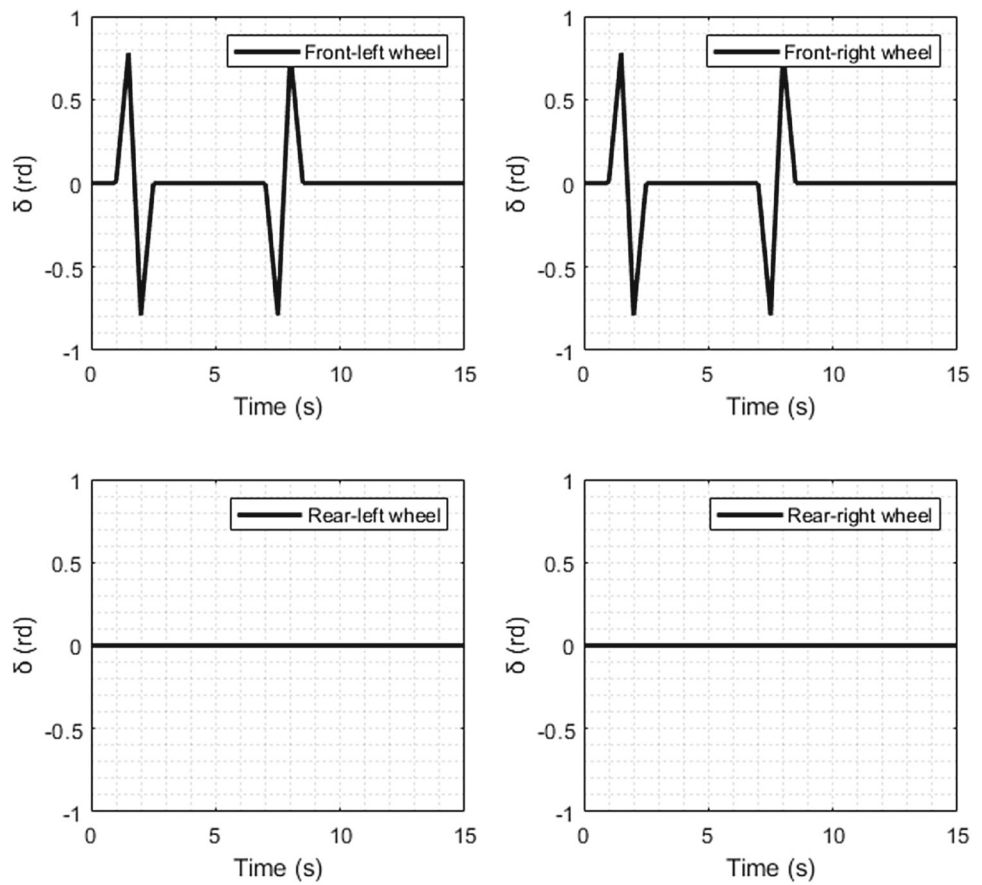
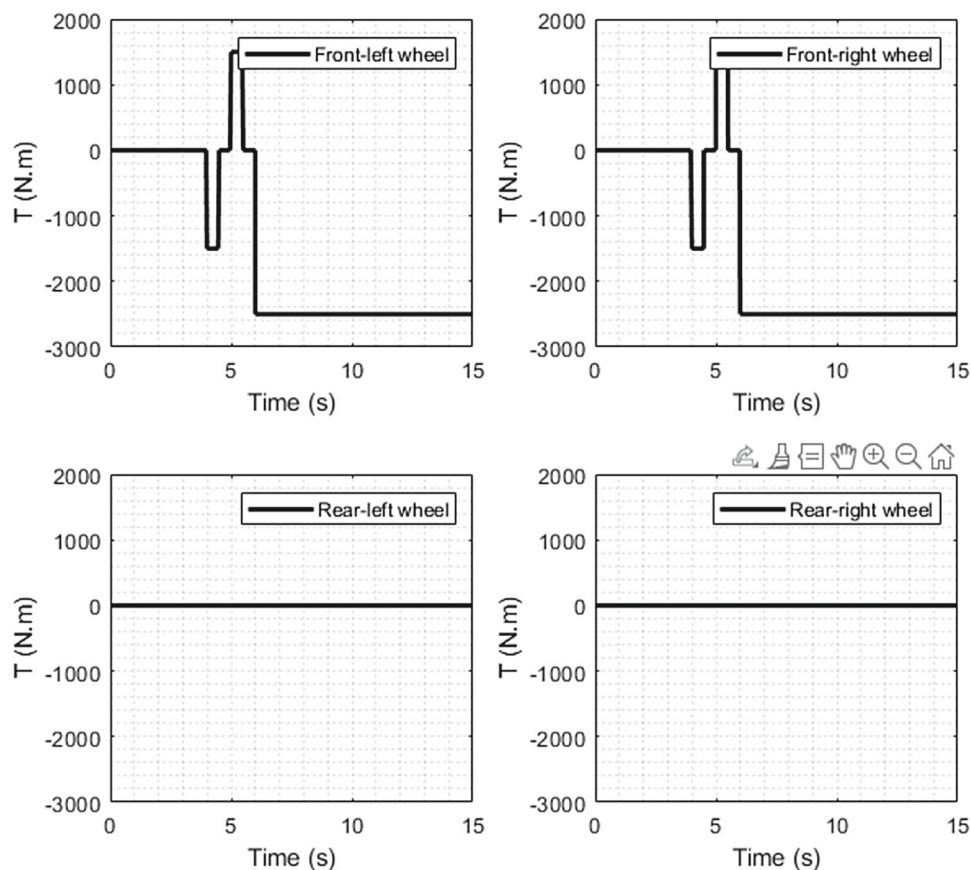


Fig. 5 Braking/accelerating torque profiles for the four wheels



This figure presents graphical profiles of the wheel/road friction coefficients for the four wheels of the vehicle. Each wheel displays its individual profile, illustrating the variation of the friction coefficient over time or distance travelled. This visualization provides a detailed insight into how the friction coefficient evolves individually for each wheel, influencing the overall performance of traction and braking.

The upper plot of Fig. 7 depicts the vehicle longitudinal acceleration. Its sign, positive or negative, matches the piecewise braking and acceleration phases, in the driving scenario, respectively. The lateral acceleration catches the steering changing alongside with the braking carried out on the μ -split track.

Figure 7 presents graphical profiles of the longitudinal and lateral accelerations of the vehicle. The curves depict the evolution of these accelerations over time or distance travelled. This visualization provides a detailed understanding of the vehicle's motion dynamics, highlighting changes in longitudinal and lateral accelerations during different driving phases.

Figure 8 illustrates the longitudinal velocity, lateral velocity and yaw rate estimates given by the sliding mode observer with initial state (66).

While facing a notably challenging assessment scenario, our study demonstrates the observer's exceptional performance in estimating key vehicle dynamics parameters throughout the simulation intervals. The accuracy of the observer shines prominently in the estimation of longitudinal velocity, lateral velocity, and yaw rate. Additionally, the observer provides highly accurate estimates even under deliberately introduced challenging initial conditions.

This figure displays the vehicle's state estimate, considering the initial condition specified in Eq. (66). The visualization offers insights into the predicted state of the vehicle based on the given initial conditions, contributing to a comprehensive understanding of the performance of the state estimation process.

These results directly contribute to a holistic understanding of the vehicle's behaviour. The observer, by providing precise estimates of key dynamic parameters, enhances the overall comprehension of the vehicle's dynamic response.

4.3 Robustness of the observer

To examine the robustness of the proposed observer, the vehicle parameters (cf. Table 1) used in the observer algorithm are 15% larger compared to their nominal values used for the vehicle truth model.

Fig. 6 The wheel/road friction coefficient for the four wheels

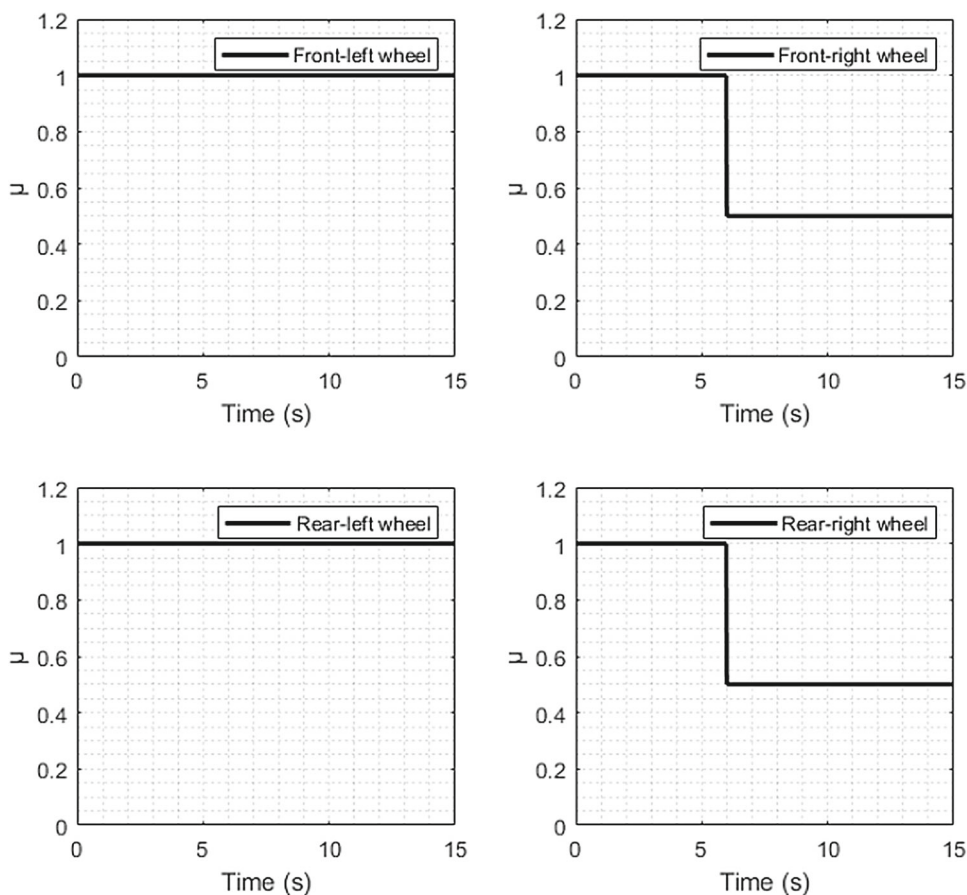


Table 2 Observer parameters for uncertain vehicle parameters

Observer parameters		
$k_{v_x} = 5$	$k_{v_y} = 0.35$	$k_r = 50$

Figure 9 illustrates the longitudinal velocity, lateral velocity and yaw rate estimates given by the sliding mode observer with initial state (66). The observer parameters are set to new values summarized in Table 2.

This figure illustrates the vehicle’s state estimate while considering the initial condition specified in Eq. (66) under uncertainties in vehicle parameters. The visualization provides insights into how the state estimation process performs in the presence of uncertainties, contributing to a comprehensive understanding of the robustness of the estimation algorithm.

Despite deviations in vehicle parameters from their nominal values, our sliding mode observer consistently provides highly accurate estimates of longitudinal velocity and yaw rate throughout all simulation intervals. The lateral velocity estimate remains remarkably acceptable, underscoring the robustness of the proposed sliding mode observer against

uncertainties in vehicle parameters. This resilience is a testament to the effectiveness of our observer in maintaining accurate estimations even under varying and uncertain vehicle conditions.

Finally, Fig. 10 illustrates the impact of uncertain tyre/road friction coefficients on our observer’s estimation. With a deliberate 20% reduction in the friction coefficient for all wheels throughout the simulation, we observe a slight influence on the lateral velocity estimate. However, it’s crucial to highlight that, despite this challenge, both the longitudinal velocity and yaw rate estimates remain remarkably accurate. Importantly, the lateral velocity results, while exhibiting a marginal effect, maintain an acceptable level of reliability. This reaffirms the observer’s robustness, demonstrating its ability to provide trustworthy estimations even under conditions of varying friction.

This figure depicts the vehicle’s state estimate considering the initial condition specified in Eq. (66) under uncertainties in both vehicle parameters and friction coefficients. The visualization provides valuable insights into the performance and robustness of the state estimation process in the face of uncertainties in these critical factors.

These results emphasize the observer’s ability to maintain accuracy even in the presence of uncertainties in vehicle

Fig. 7 Longitudinal and lateral accelerations

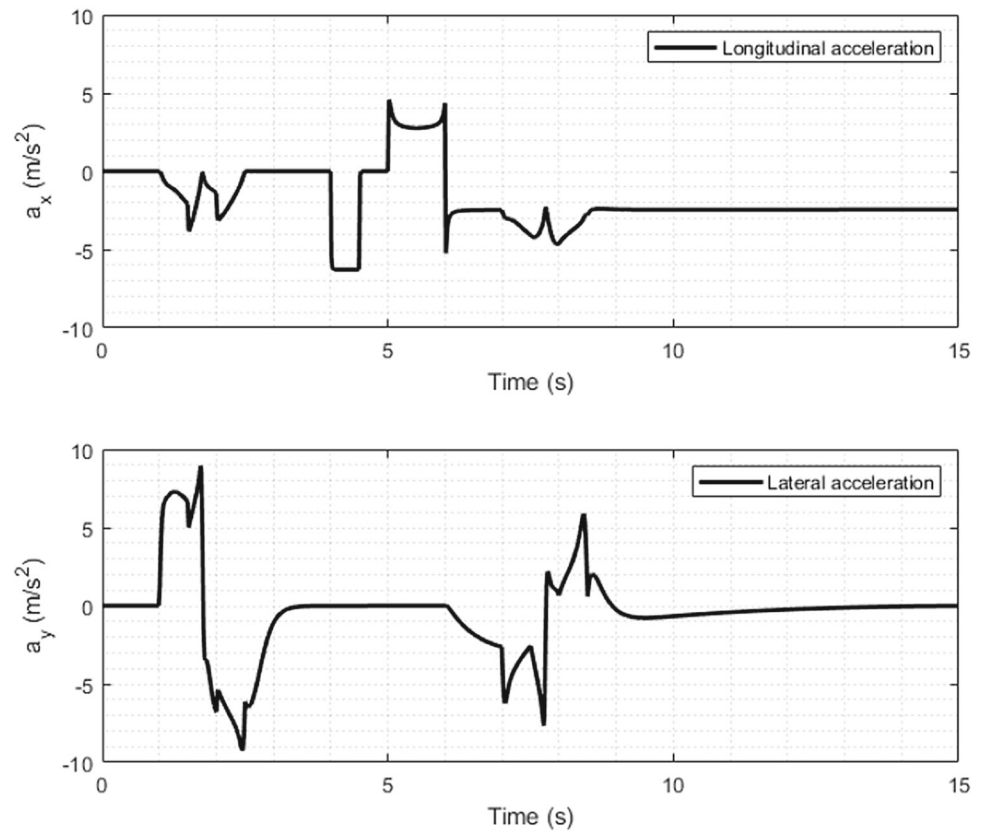


Fig. 8 Vehicle state estimate with initial condition (66)

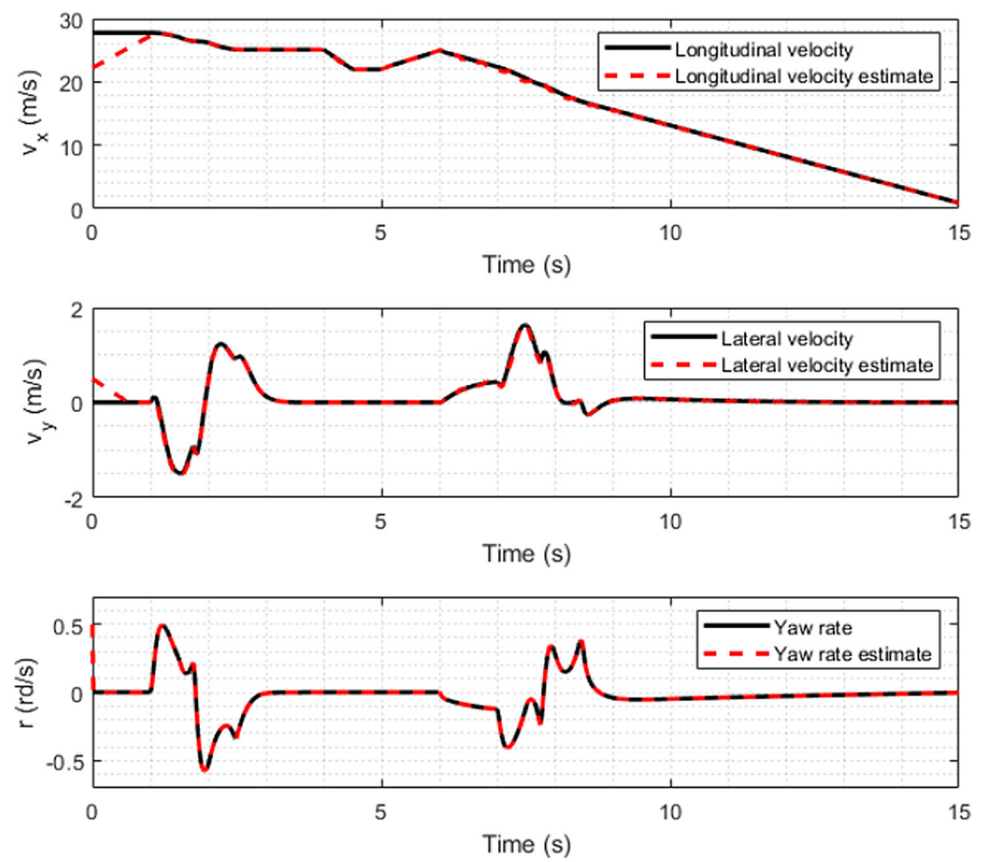
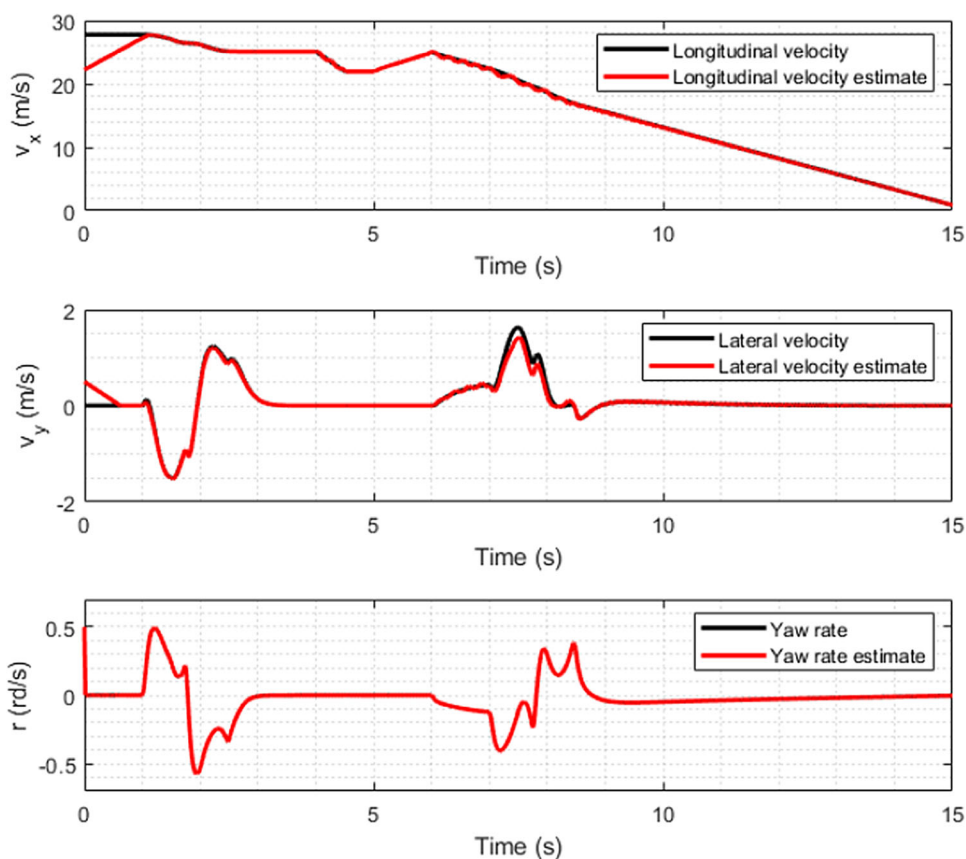


Fig. 9 Vehicle state estimate with initial condition (66) under vehicle parameters uncertainties



parameters and the friction coefficient, reinforcing its contribution to the overall control system.

5 Conclusion and perspectives

In this study, we introduced a nonlinear sliding mode observer. Our observer design assumes the availability of measurements such as longitudinal acceleration, lateral acceleration, yaw rate, wheel angular velocities, and wheel steering angle. Based on a planar double-track vehicle model, this design incorporates the Pacejka nonlinear tire model to evaluate friction forces.

The stability analysis of the observer has been thoroughly conducted using a quadratic Lyapunov function in conjunction with the Sylvester criterion. We assessed the robustness of the observer against uncertainties related to vehicle parameters and tire/road friction coefficient.

Sufficient conditions for observer gains have been established, and their numerical values have been defined for simulation, demonstrating promising results. While the driving scenario used for observer evaluation is highly challenging, the state estimation proves to be highly accurate.

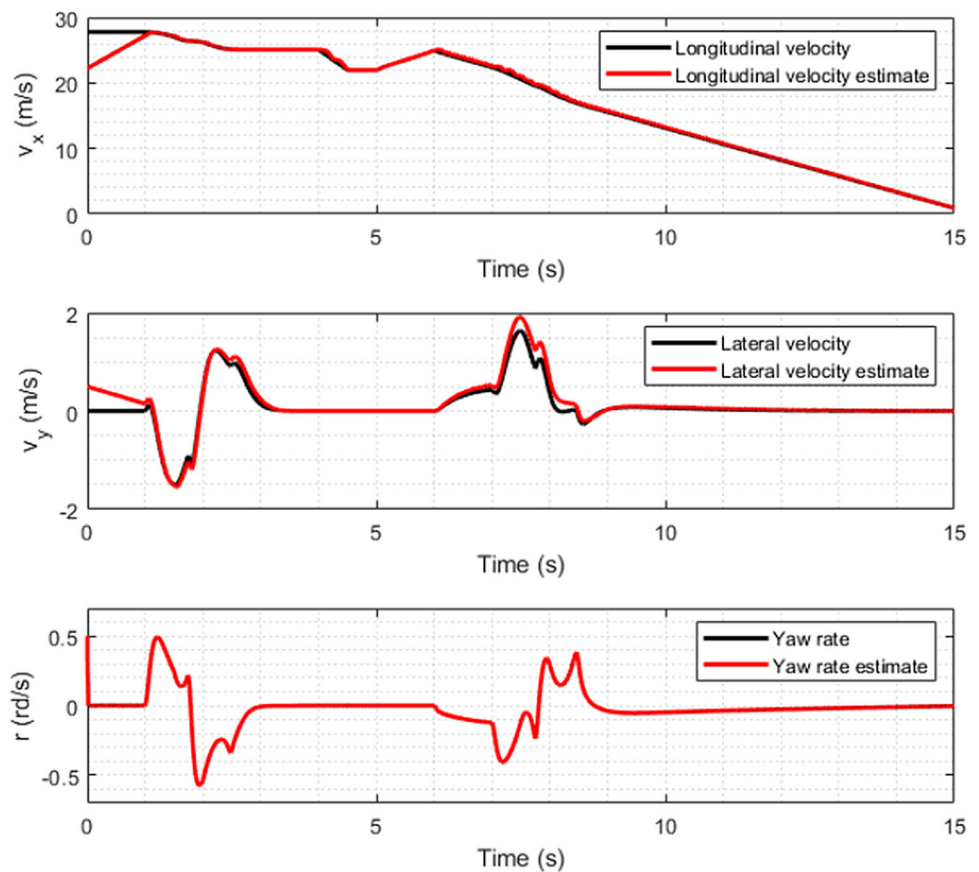
The robustness of the proposed observer against uncertainties has been validated through numerical simulation. We

conclude that longitudinal velocity and yaw rate are relatively insensitive to vehicle parameters and tire-road friction coefficient uncertainties. However, lateral velocity is slightly affected when the friction coefficient is not well known, although this limitation can be overcome with online estimation.

In summary, our nonlinear sliding mode observer emerges as a robust and effective solution for vehicle state estimation, providing reliable performance even in demanding driving conditions. Looking ahead, several promising research directions emerge to enhance the robustness and applicability of the proposed sliding mode observer. An intriguing avenue involves exploring the integration of additional filtering algorithms, such as the Kalman filter, to further mitigate potential noise impacting acceleration and rotation speed measurements. The utilization of these advanced filtering algorithms could contribute to refining the observer’s precision, especially in challenging driving scenarios.

Furthermore, a natural extension of this research would involve investigating the practical implementation of the observer in advanced control algorithms, particularly in anti-lock braking systems (ABS) and traction control systems (ASR). By integrating this observer into these systems, we could fully leverage its precision and robustness capabilities

Fig. 10 Vehicle state estimate with initial condition (66) under vehicle parameters and friction coefficient uncertainties



to enhance vehicle stability and performance in diverse conditions. This synergy between the sliding mode observer and advanced control systems could open new perspectives for safer and more responsive vehicles.

Acknowledgements We would like to express our sincere thanks to our family for their constant support throughout our research journey. We also extend our gratitude to our supervisor, Mohammed Bakhti, for his guidance, valuable insights, and invaluable contribution to this research. We appreciate the collaborative discussions and idea exchanges with our research team. We acknowledge our institution for providing the conducive research environment and necessary resources.

Author contributions BMH was first author, doctoral student, contributed to the research design, model implementation, data collection and analysis, and article writing. MB was second author, supervisor, provided guidance, technical advice, and extensive expertise throughout the research and article writing process.

Funding This research was self-funded, with no external grants or scholarships.

Data availability The data used in this research are based on simulations conducted using MATLAB software.

Declarations

Competing interests We declare no Competing interests regarding this research. The authors have no financial or personal interests that could influence the results or interpretation of the study.

References

- Ryu J, Gerdes JC (2004) Integrating inertial sensors with global positioning system (GPS) for vehicle dynamics control. *J Dyn Syst Meas Control* 126(2):243–254
- Imsland L, Johansen TA, Fossen TI, Grip HF, Kalkkuhl C, Suissa A (2006) Vehicle velocity estimation using nonlinear observers. *Automatica* 42(12):2091–2103
- Bevly DM, Ryu J, Gerde DM (2006) Integrating INS sensors with GPS measurements for continuous estimation of vehicle sideslip, roll, and tire cornering stiffness. *IEEE Trans Intell Transp Syst* 7(4):483–493
- Jalali M, Hashemi E, Khajepour A, Chen S, Litkouhi B (2017) Integrated model predictive control and velocity estimation of electric vehicles. *Mechatronics* 46:84–100
- Wenzel TA, Burnham KJ, Blundell MV, Williams RA (2006) Dual extended Kalman filter for vehicle state and parameter estimation. *Veh Syst Dyn* 44(2):153–171
- Tong L. An approach for vehicle state estimation using extended Kalman filter. In: Xiao T, Zhang L, Ma S (eds), *System simulation and scientific computing*. ICSC 2012. Communications in computer and information science, vol 326. Springer, Berlin

7. Reina G, Paiano M, Blanco-Claraco JL (2017) Vehicle parameter estimation using a model-based estimator. *Mech Syst Signal Process* 87(B):227–241
8. Reina G, Messina A (2019) Vehicle dynamics estimation via augmented extended Kalman filtering. *Measurement* 133:383–395
9. Huang X, Wang, J (2013) Robust sideslip angle estimation for lightweight vehicles using smooth variable structure filter. In: *Proceedings of the ASME dynamic systems and control conference*. Palo Alto, California, USA, pp 21–23
10. El Youssfi N, Oudghiri M, El Bachtiri R (2019) Vehicle lateral dynamics estimation using unknown input observer. *Procedia Informatique Tome* 148:502–511
11. Antonov S, Fehn A, Kugi A (2011) Unscented Kalman filter for vehicle state estimation. *Veh Syst Dyn* 49(9):1497–1520
12. Wielitzka M, Dagen M, Ortmaier T (2015) State estimation of vehicle's lateral dynamics using unscented Kalman filter. In: *Proceedings of the IEEE conference on decision and control*; (February Issue), pp 5015–5020
13. Jiang G, Liu L, Guo C, Chen J, Muhammad F, Miao X (2017) A novel fusion algorithm for estimation of the side-slip angle and the rolling angle of a vehicle with optimized key parameters. *Proc IMechE Part D J Automob Eng* 231:161–174
14. Cheng S, Li L, Chen J (2018) Fusion algorithm design based on adaptive SCKF and integral correction for side-slip angle observation. *IEEE T Ind Electron* 65:5754–5763
15. Chen X, Li S, Li L, Zhao W, Cheng S (2022) Longitudinal-lateral-cooperative estimation algorithm for vehicle dynamics states based on adaptive-square-root-cubature-Kalman-filter and similarity-principle. *Mech Syst Signal Process* 176:109162
16. Zhang H, Zhang G, Wang J (2016) H_∞ observer design for LPV systems with uncertain measurements on scheduling variables: application to an electric ground vehicle. *IEEE ASME T Mech* 21:1659–1670
17. Zhang H, Wang J (2017) Active steering actuator fault detection for an automatically-steered electric ground vehicle. *IEEE T Veh Technol* 66:3685–3702
18. Stephant J, Charara A, Meizel D (2004) Virtual sensor: application to vehicle sideslip angle and transversal forces. *IEEE T Ind Electron* 51:278–289
19. Das P, Das S, Upadhyay RK, Das P (2020) Optimal treatment strategies for delayed cancer-immune system with multiple therapeutic approach. *Chaos Solitons Fractals* 136:109806
20. Das P, Das S, Das P, Rihan FA, Uzuntarla M, Ghosh D (2021) Optimal control strategy for cancer remission using combinatorial therapy: a mathematical model-based approach. *Chaos Solitons Fractals* 145:110789
21. Das S, Das P, Das P (2020) Dynamics and control of multidrug-resistant bacterial infection in hospital with multiple delays. *Commun Nonlinear Sci Numer Simul* 89:105279
22. Pacejka HB (2002) *Tire and vehicle dynamics*. SAE, Warrendale
23. Deur J, Kranjcevic N, Hofmann O, Asgari J, Hrovat D (2009) Analysis of lateral tyre friction dynamics. *Vehicle Syst Dyn* 47:831–850
24. Uil T (2007) *Tyre models for steady-state vehicle handling analysis*. Master's Thesis, Eindhoven University of Technology, Department of Mechanical Engineering, Dynamics and Control Group, Eindhoven
25. Dugoff H, Fancher P, Segel L. An analysis of tire traction properties and their influence on vehicle dynamic performance. SAE technical paper 700377. 1970.
26. Rajesh R (2012) *Vehicle dynamics and control*, 2nd edn. Springer, Berlin
27. Kiencke U, Nielsen L (2005) *Automotive control system for engine, driveline, and vehicle*, 2nd edn. Springer, Berlin
28. Bakker E, Nyborg L, Pacejka HB (1987) Tire modelling for use in vehicle dynamics studies. SAE Technical Paper 870421
29. Li B, Du H, Li W, Zhang B (2019) Non-linear tyre model-based non-singular terminal sliding mode observer for vehicle velocity and side-slip angle estimation. *Proc Inst Mech Eng Part D J Automob Eng* 233(1):38–54
30. Singh KB, Arat MA, Taheri S (2013) An intelligent tire based tire-road friction estimation technique and adaptive wheel slip controller for antilock brake system. *J Dyn Syst Meas Control*. 135(3):031002
31. Guo H, Cao D, Chen H, Lv C, Wang H, Yang S (2018) Vehicle dynamic state estimation: state of the art schemes and perspectives. *IEEE/CAA J Autom Sin* 5(2):418–431
32. Dugoff H, Fancher PS, Segel L (1970) An analysis of tire traction properties and their influence on vehicle dynamic performance. *SAE Trans* 79:341–366
33. Lee H, Taheri S (2017) Intelligent tires—a review of tire characterization literature. *IEEE Intel Transp Syst Magn* 9(2):114–135

Springer Nature or its licensor (e.g. a society or other partner) holds exclusive rights to this article under a publishing agreement with the author(s) or other rightsholder(s); author self-archiving of the accepted manuscript version of this article is solely governed by the terms of such publishing agreement and applicable law.